Supporting Information For

Simultaneous analysis of dopamine and homovanillic acid by high-performance liquid chromatography with wall-jet/thin-layer electrochemical detection

Yaping Zhou,[a] Hongling Yan,[a] Qingji Xie,[a,*] Siyu Huang,[a] Jiali Liu,[a] Zou Li,[a] Ming Ma,[a] and Shouzhuo Yao[a,b]

[a] *Key Laboratory of Chemical Biology and Traditional Chinese Medicine Research (Ministry of Education), College of Chemistry and Chemical Engineering, Hunan Normal University, Changsha 410081, P. R. China*

[b] *State Key Laboratory of Chemo/Biosensing and Chemometrics, College of Chemistry and Chemical Engineering, Hunan University, Changsha 410082, P. R. China*

* Corresponding author. Tel./Fax: +86 731 88865515.
E-mail: xieqj@hunnu.edu.cn (Q. Xie).

Contents

1. Procedures for CV Experiments at area-increased GCEs

Before electrochemical experiments, the GCE was polished on a polishing pad with 0.05 μm alumina slurry, rinsed with water. Subsequently it was ultrasonicated thoroughly in ethanol and water respectively, and dried with nitrogen blowing. A rough electrode surface was achieved by electrochemically etching according to a previous paper.[1] The electrode was treated in 0.10 M NaOH at 1.8 V and then reduced at -1.0 V. We could obtain the nanoporous GCEs of varying cavity density by changing the time of electrochemical treatment. The GCE electrodeposited with AuNPs was carried out in 0.50 M aqueous H_2SO_4 containing 2.00 mM $HAuCl_4$ by potentiostatic electrolysis at 0 V (stepped from 1.1 V) for various time.[2] To obtain the MWCNTs modified GCE, the purified MWCNTs were treated with a mixture of nitric acid and sulfuric acid (v/v = 1:3),[3] and then dispersed in water with ultrasonic agitation. A 2 μL aliquot of the MWCNTs suspension was dropped on the freshly polished electrode surface and the solvent was evaporated at room temperature, resulted in a MWCNTs modified GCE.

2. Bulk-electrolysis and chemical oxidation of HVA

Bulk electrooxidation was carried out with a glassy carbon plate electrode (2.2 cm × 1.4 cm) in stirred 0.01 M ammonium acetate solution (pH 6.70) initially containing 100 μM HVA and the CV detection (100 mV s^{-1}) was performed with a glassy carbon disk electrode (3 mm in diameter) in the bulk-electrolysis bath. Chemical oxidation of HVA was conducted by adding 1.45 mg L^{-1} horseradish peroxidase (HRP, 500 U mg^{-1}) and 0.72 mM hydrogen peroxide into stirred 0.01 M ammonium acetate solution (pH 6.70) containing 100 μM HVA.

3. Fluorescent and CV experiments for HVA-electrooxidation mechanism

According to the previous report, HVA could be chemically oxidized to its dimer, a highly

fluorescent compound.[4, 5] So we conducted fluorometric assay to confirm whether the dimer product was produced in the process of HVA electrooxidation or not, and the results are shown in Fig. S-12. We found that HVA before and after electrooxidation has the maximum emission wavelength merely at 323 nm, which decreased after 30 min electrolysis. However, the emission peak after adding horseradish peroxidase and hydrogen peroxide into the HVA-electrooxidation bath shifted to 434 nm, which is identical to the case of directly mixing horseradish peroxidase, hydrogen peroxide and HVA without electrooxidation, also in acceptable accordance with the fluorescent property of chemical-oxidation products of HVA reported in literature (425 nm emission, 315 nm excitation, different buffer and pH).[4, 5] Hence, we can come to the conclusion that the products of HVA electrooxidation do not have the fluorescence of chemical-oxidation product of HVA until the addition of the chemical oxidant, namely, there is no HVA dimer produced in the process of HVA electrooxidation.

In addition, we also studied the cyclic voltammetric behavior of HVA chemical-oxidation products. In Fig. S-13, we found that a pair of redox peaks appeared at 0.17 V/0.10 V after the addition of horseradish peroxidase and hydrogen peroxide into HVA, and the approximate formal potential of the chemical-oxidation products ((0.17+0.10)/2=0.14 V) was negative than that of the electrooxidation products ((0.25+0.18)/2=0.22 V), indicating that chemical-oxidation products of HVA are different from the electrooxidation products. Also, after mixing the chemical-oxidation and electrooxidation products, we obtained a pair of wider redox peaks and its formal potential changed to (0.22+0.14)/2=0.18 V, being due to a combination of the CV behaviors of chemical-oxidation and electrooxidation products.

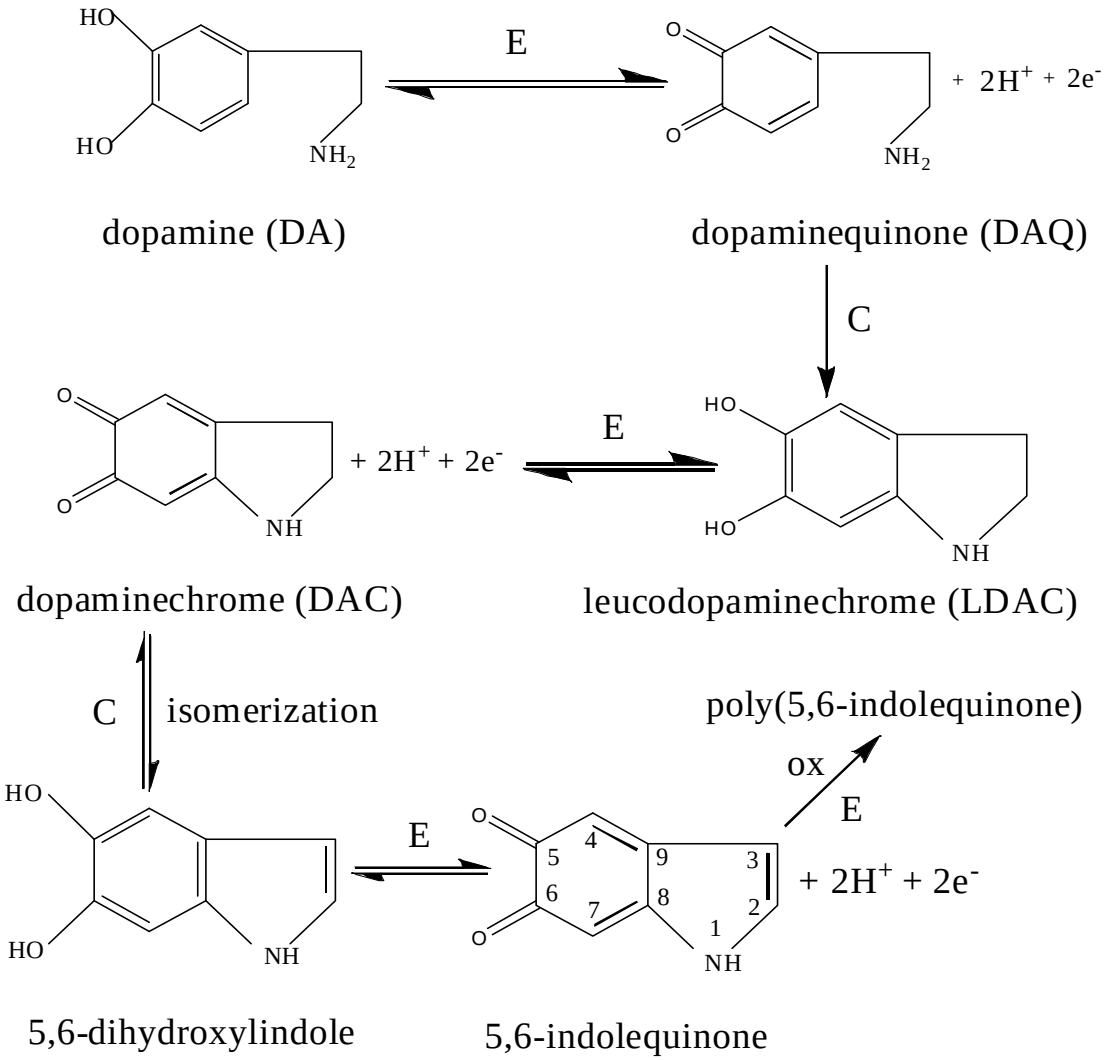

Scheme S-1. A reported ECECEE mechanism for DA electrooxidation and polymerization in aqueous solution.[6]

Table S-1. Data for the cyclic voltammetric experiments given in **Fig. S-1**

Instrument recording scale ($A\ V^{-1}$)	Oxidation peak current (μA)	Noise (nA)	Signal-to-noise ratio (S/N)
2×10^{-4}	17.3	150	115
1×10^{-4}	17.5	75	233
1×10^{-5}	17.2	25	688

Table S-2. Data for the repeatability experiments given in **Fig. S-3**

Experiment no.	Peak current (μA)[a]	RSD (%)
1st	1.20 ± 0.02	1.67
2nd	1.21 ± 0.04	3.31
3rd	1.21 ± 0.03	2.48

[a] Average value ± S.D. (n = 3).

Table S-3. Parameters of linear regression analysis and LODs obtained by different HPLC detectors.

Analyte	Regression equation[a]	Linear range (μM)	R^2	LOD (nM)
Self-fabricated ECD				
DA	$y = 22.6x - 4.29$	0.01 – 100	0.9999	1.1
HVA	$y = 19.6x + 2.40$	0.01 – 100	0.9999	0.7
UV-detection				
DA	$y = 5.22 \times 10^2 x - 52.0$	0.10 – 100	0.9998	21
HVA	$y = 5.39 \times 10^2 x + 163$	0.10 – 100	0.9998	15
Commercial ECD				
DA	$y = 1.09 \times 10^4 x - 370$	0.10 – 10.0	0.9994	12
HVA	$y = 1.54 \times 10^4 x + 725$	0.04 – 10.0	0.9988	8

[a] y and x represent the peak height (nA in self-fabricated ECD and μV in UV-detection and commercial ECD) and the concentration of the analytes (μM), respectively.

Table S-4. Comparison of LODs for DA and HVA determined by some typical methods

Analyte	Analytical method	LOD (nM)	Reference
DA	HPLC-ECD (amperometric detection)	1.1	This work
	HPLC-ECD (amperometric detection)	22	[7]
	HPLC-ECD (MWCNT-GCE)	2.5	[8]
	HPLC-fluorescence detection	70	[9]
	HPLC-mass spectrometry	44	[10]
	HPLC-chemiluminescence	2	[11]
	CE-UV	700	[12]
	CE-MS	1200	[12]
	DPV (pyrolytic carbon film electrode)	40	[13]
	DPV (hollow nitrogen-doped carbon microspheres/GCE)	20	[14]
	DPV (methylene blue-MWCNTs/GCE)	200	[15]
HVA	HPLC-ECD (amperometric detection)	0.7	This work
	HPLC-ECD (coulometric detection)	0.5	[16]
	HPLC-ECD (MWCNT-GCE)	1.25	[17]
	HPLC-mass spectrometry	300	[18]
	HPLC-chemiluminescence	140	[11]
	CE-UV	1800	[19]

Table S-5. Intra-day and inter-day variability of DA and HVA detection using our ECD

Analyte	Concentration (μM)	RSD (%)	
		Intra-day (n = 5)	Inter-day (n = 3)
DA	0.50	1.45	3.98
	5.00	2.47	4.45
	50.0	2.62	4.62
HVA	0.50	1.79	3.80
	5.00	2.35	4.24
	50.0	2.89	4.85

Table S-6. Results for DA and HVA determination in human urine samples with our HPLC-ECD[a]

Sample No.	DA				HVA			
	Original (μM)	Added (μM)	Found (μM)	Recovery (%)	Original (μM)	Added (μM)	Found (μM)	Recovery (%)
1	0.11±0.02	2.00	1.91±0.02	95.5	1.26±0.05	10.0	9.24±0.38	92.4
2	0.68±0.03	2.00	1.96±0.03	98.0	1.87±0.26	10.0	10.36±0.45	103.6
3	0.31±0.02	2.00	2.03±0.02	101.5	1.51±0.14	10.0	9.76±0.34	97.6

[a] Data expressed as mean value ± S.D. (n = 3).

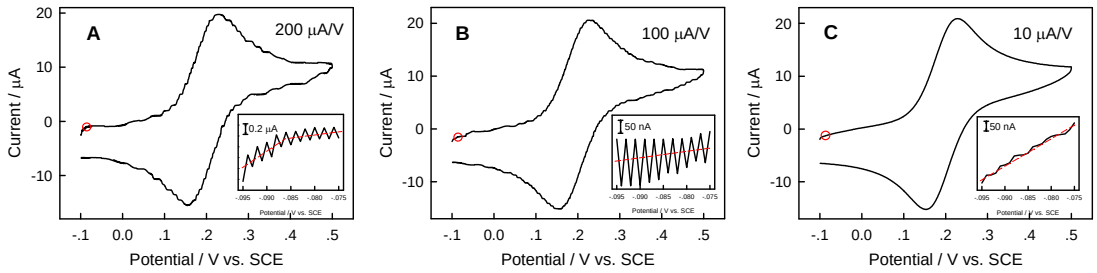

Fig. S-1. Cyclic voltammograms of 0.10 M aqueous Na_2SO_4 containing 2.00 mM ferrocyanide on GCE (3 mm in diameter) at different recording scales. Scan rate: 50 mV s^{-1}. Insets are the magnification of the red circled parts, with the red dashed central line shown. Here, the scale of 2.0×10^{-4} A V^{-1} was used to record the current from 2×10^{-3} to 2×10^{-7} A with an apparent noise of 1.5×10^{-7} A, the scale of 1.0×10^{-4} A V^{-1} was used to record the current from 1×10^{-3} to 1×10^{-7} A with an apparent noise of 7.5×10^{-8} A, and the scale of 1.0×10^{-5} A V^{-1} was used to record the current from 1×10^{-4} to 1×10^{-8} A with an apparent noise of 2.5×10^{-8} A. See Table S1 for data details, which reveals that the smallest scale of 1.0×10^{-5} A V^{-1} here yields the best signal-to-noise ratio. From this example, we believe that any scale of any instrument can precisely record data merely covering ca. 4 orders of magnitude (virtually, a 0.1-mg-precision analytical balance and a ton-scale weighbridge have their different data-recording precision), thus accurately selecting the instruments' data-recording scale and reducing the signal-background to achieve a smaller data-recording scale are very important in quantitative instrumental analysis, namely, one should always pay the greatest attention to the balance among response-signal, signal-background and noise in quantitative instrumental analysis.

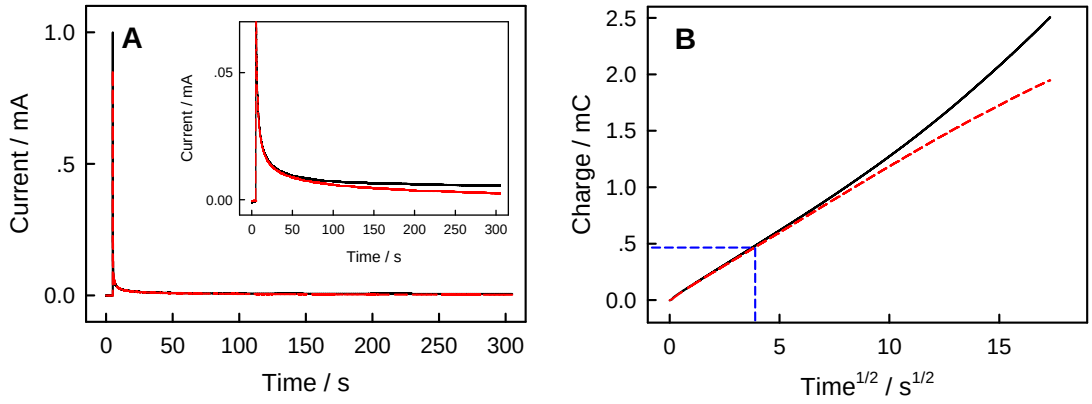

Fig. S-2. (A) Chronoamperometric curves and (B) the electrolysis charge versus square root of time curves of 2.00 mM ferrocyanide in 0.10 M Na_2SO_4 aqueous solution at GCE (5 mm in diameter) conducted in conventional electrolysis cell (black solid curve) and our ECD cell (red dashed curve). Applied potential: 0.50 V. Here, we applied 0.50 V to electrolyze the 2.00 mM ferrocyanide in 0.10 M Na_2SO_4 aqueous solution in conventional electrolysis cell (semi-infinite diffusion) and our ECD cell (thin-layer diffusion), respectively. The electrolysis charge versus square root of time curves should be overlapped at first and then deviate from each other after a critical time (t_c). The critical time (t_c) can be roughly taken as the time just reaching an exhausted electrolysis of ferrocyanide in the thin layer, and the charge at t_c can thus be used to roughly estimate the thick-layer thickness. Based on the Faraday law, we can estimate the thin-layer thickness by $Q = zFn = zFcAl$, where Q in C is the electrolysis charge; z is the number of electrons transferred (here z=1); F is the Faraday constant (96485.33 C mol^{-1}); n in mol is the amount of exhaustedly electrolyzed ferrocyanide; c in mol mL^{-1} is the concentration of ferrocyanide; A is the electrode area (here A= 1.96 × 10^{-1} cm^2); and l in cm is the thin-layer thickness. Here, we obtain the average Q as 460 μC and the l is calculated to be ca. 120 ± 20 μm in three runs.

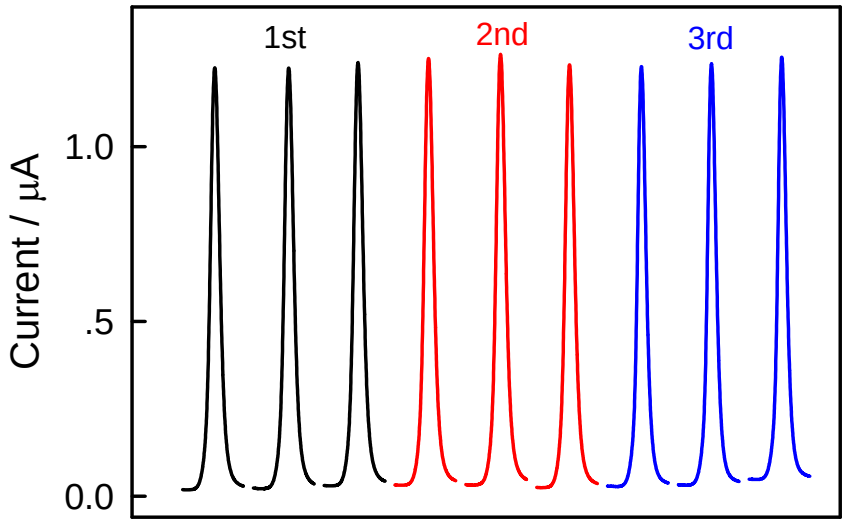

Fig. S-3. Chromatograms of 50.0 μM DA obtained at bare GCE (5 mm in diameter) by repeating the GCE-plexiglass plate contact 3 times (3 runs of DA analysis every time). Shim-pack VP-ODS (5 μm, 150 × 4.6 mm) column, 0.10 mol L^{-1} acetate buffer (pH 4.00) containing 0.42 mM 1-octanesulfonic acid sodium and 10% (v/v) methanol as mobile phase, 1 mL min^{-1} flow rate, injected volume: 20.0 μL, applied potential: 0.70 V.

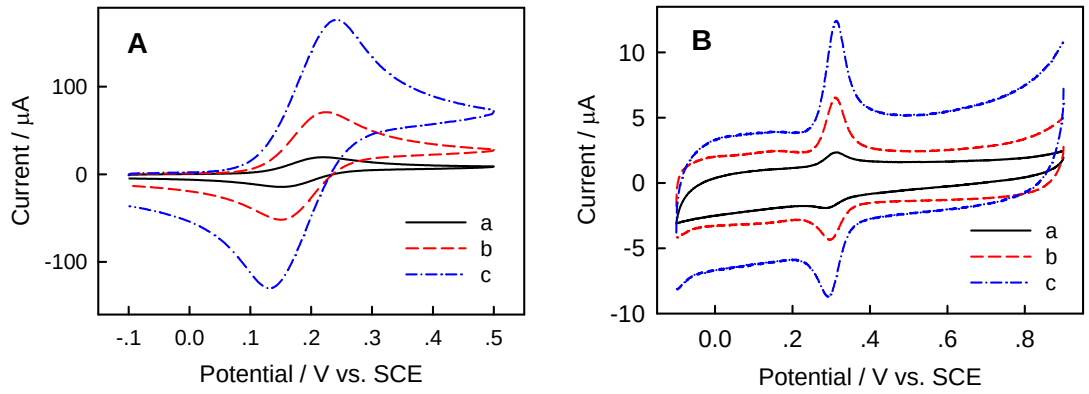

Fig. S-4. Cyclic voltammograms in 0.10 M Na_2SO_4 aqueous solution containing 2.00 mM ferrocyanide (A) or 0.10 M acetate buffer (pH 4.00) containing 10.0 μM DA (B) at GCEs of diameters of 3 mm (a, black solid curves), 5 mm (b, red dashed curves) and 9 mm (c, blue dashed dotted curves). Scan rate: 100 mV s^{-1}.

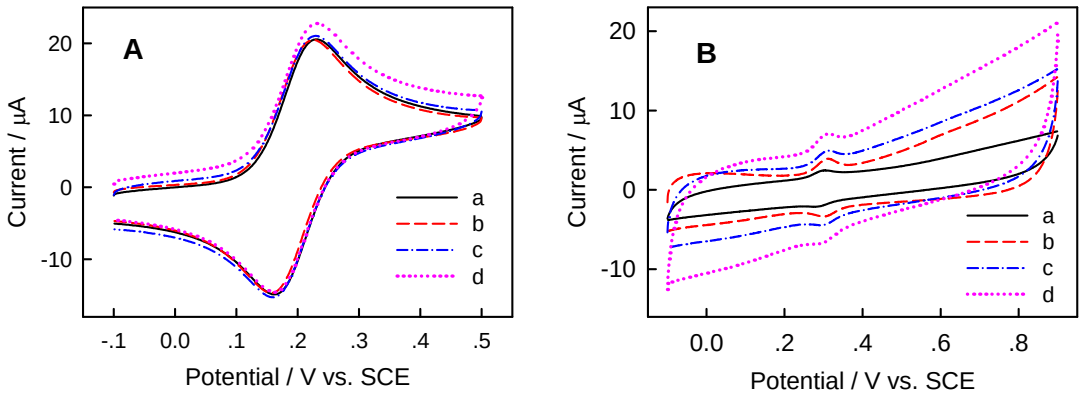

Fig. S-5. Cyclic voltammograms in 0.10 M Na_2SO_4 aqueous solution containing 2.00 mM ferrocyanide (A) or 0.10 M acetate buffer (pH 4.00) containing 10.0 μM DA (B) at the electrochemically etched nanoporous GCEs by oxidization at 1.8 V followed by reduction at -1.0 V in 0.10 M NaOH. (a) Untreated GCE (black solid curves), (b) 1.8 V oxidization for 3 min and -1.0 V reduction for 1 min (red dashed curves), (c) 1.8 V oxidization for 6 min and -1.0 V reduction for 2 min (blue dashed dotted curves), (d) 1.8 V oxidization for 9 min and -1.0 V reduction for 3 min (pink dotted curves). Scan rate: 100 mV s^{-1}. Such an electrochemical etching to form a nanoporous GCE was reported previously by Liu et al.[1]

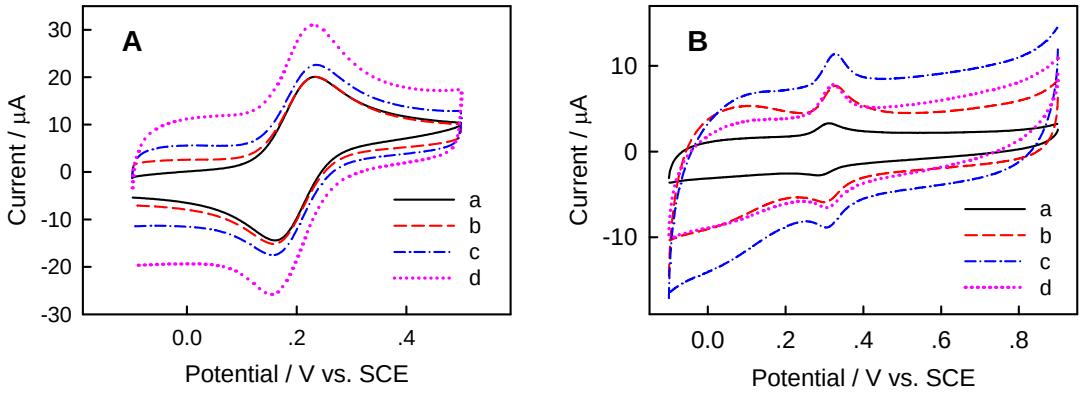

Fig. S-6. Cyclic voltammograms in 0.10 M Na_2SO_4 aqueous solution containing 2.00 mM ferrocyanide (A) or 0.10 M acetate buffer (pH 4.0) containing 10.0 μM DA (B) at the GCEs cast-coated with 0 (a, black solid curves), 1.00 mg mL^{-1} (b, red dashed curves), 2.00 mg mL^{-1} (c, blue dashed dotted curves), or 3.00 mg mL^{-1} MWCNTs (d, pink dotted curves). Scan rate: 100 mV s^{-1}.

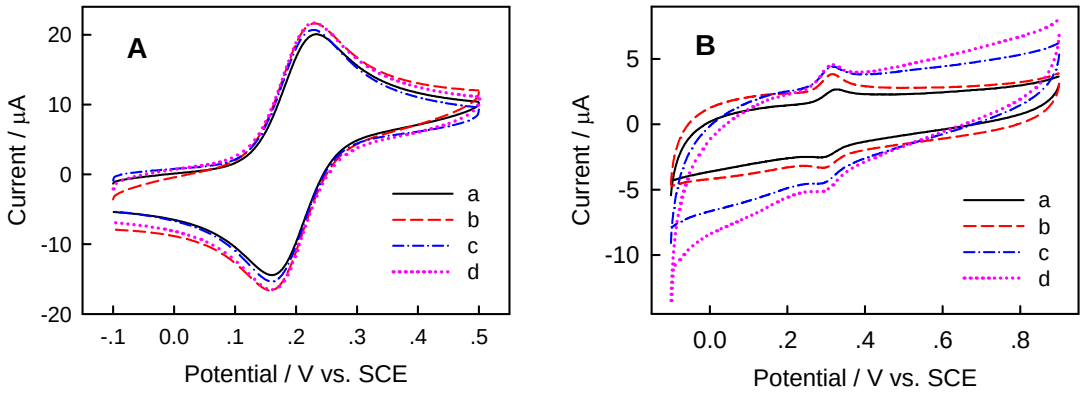

Fig. S-7. Cyclic voltammograms in 0.10 M Na_2SO_4 aqueous solution containing 2.00 mM ferrocyanide (A) or 0.10 M acetate buffer (pH 4.0) containing 10.0 μM DA (B) at the GCEs modified with electrodeposited Au nanoparticles. Scan rate: 100 mV s^{-1}. The Au nanoparticles were electrodeposited at the GCE by potentiostatic electrolysis at 0 V for 0 s (a, black solid curves), 75 s (b, red dashed curves), 150 s (c, blue dashed dotted curves), or 300 s (d, pink dotted curves) in 0.50 M aqueous H_2SO_4 containing 2.00 mM $HAuCl_4$.

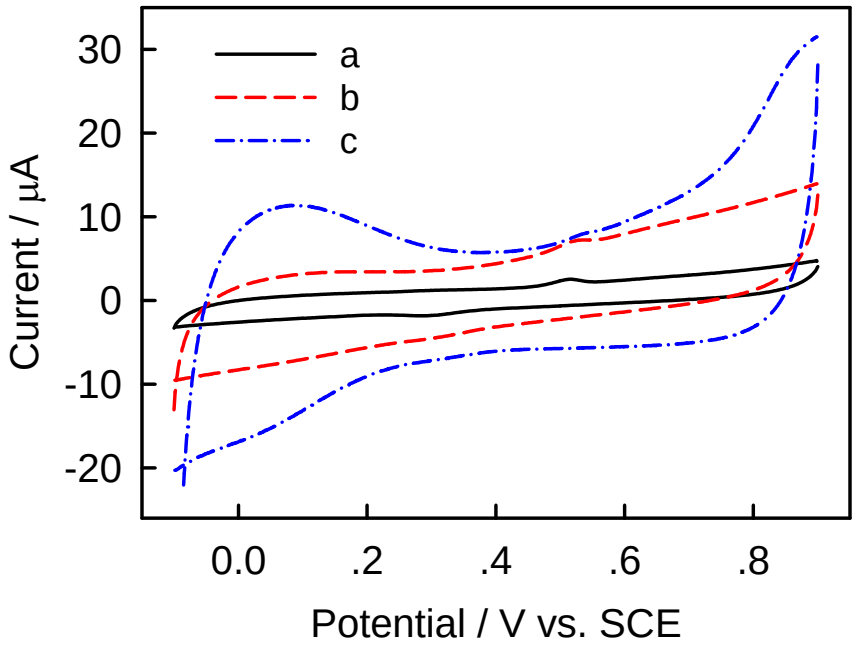

Fig. S-8. The 1st cycles of cyclic voltammograms of 0.10 M acetate buffer (pH 4.00) containing 10.0 μM HVA at the bare GCE (a, black solid curve), nanoporous GCE electrochemically pretreated in 0.10 M NaOH by oxidization at 1.8 V for 6 min followed by reduction at -1.0 V for 2 min (b, red dashed curve) and the GCE cast-coated with 2.00 mg mL^{-1} MWCNTs (c, blue dashed dotted curve). Scan rate: 100 mV s^{-1}.

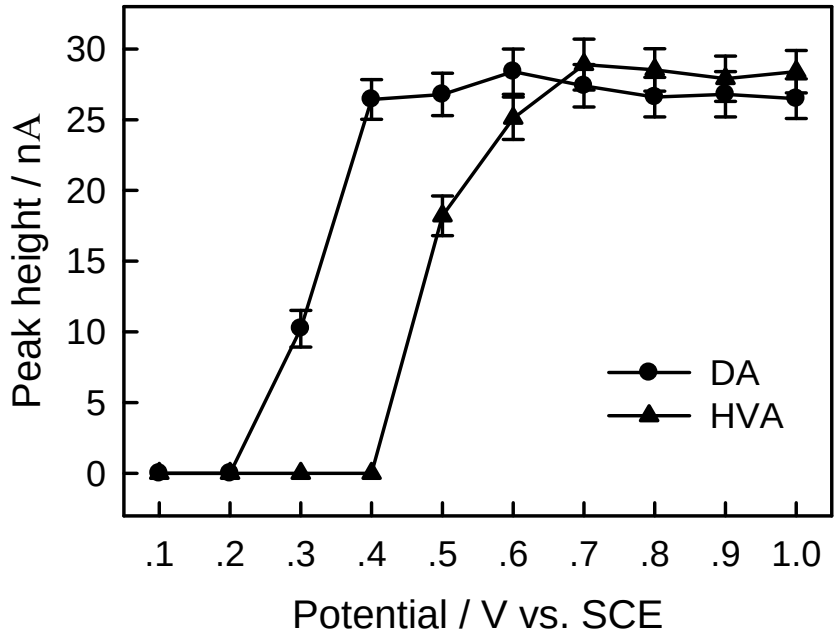

Fig. S-9. The hydrodynamic voltammograms of DA and HVA. Shim-pack VP-ODS (5 μm, 150 × 4.6 mm) column, 0.10 mol L^{-1} acetate buffer (pH 4.00) containing 0.42 mM 1-octanesulfonic acid sodium and 10% (v/v) methanol as mobile phase, 1.0 mL min^{-1} flow rate, injected 20.0 μL standard mixture of analyte solutions with $c = 2.00 \times 10^{-6}$ mol L^{-1} each. GCE (3 mm in diameter) served as the working electrode.

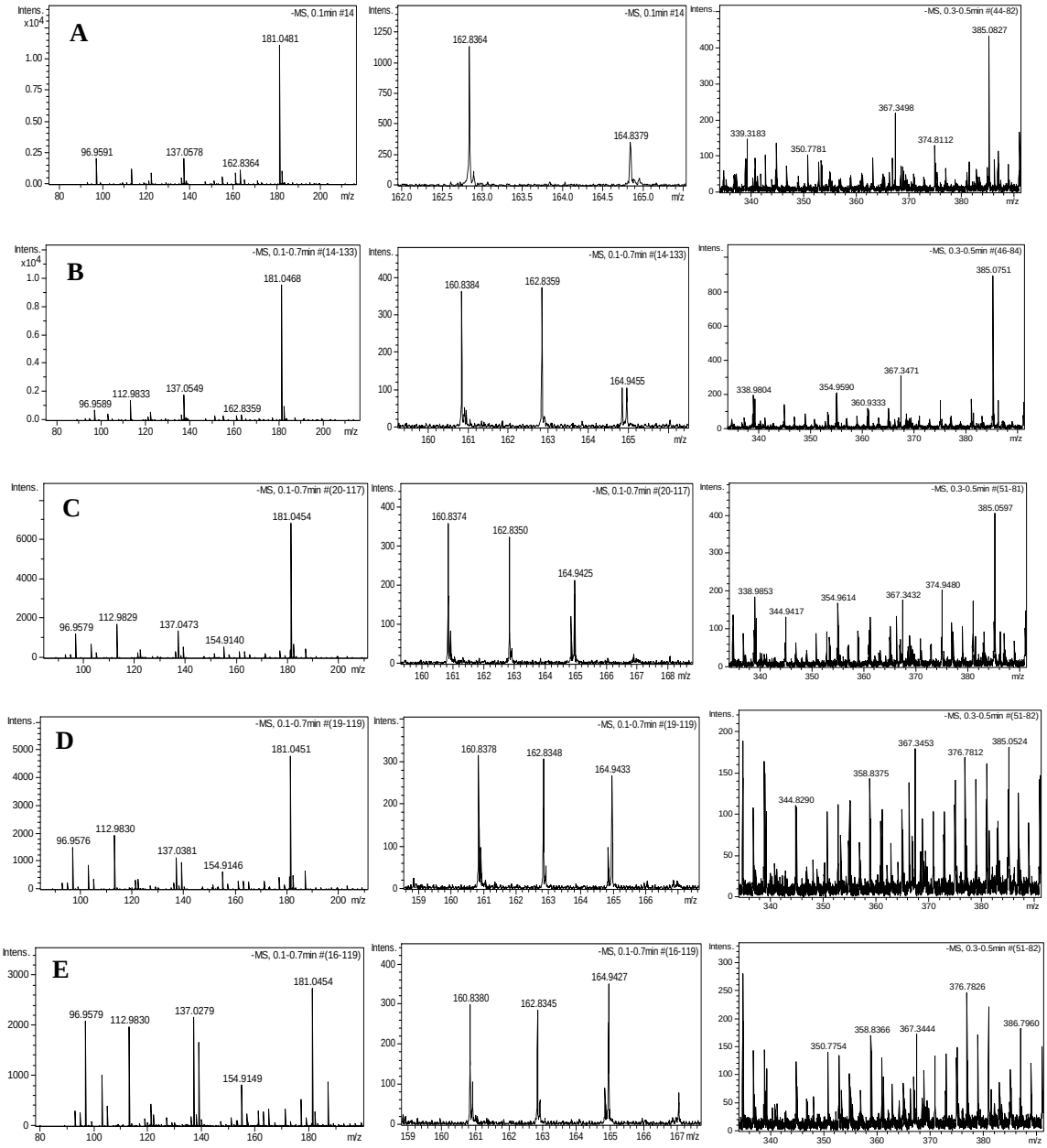

Fig. S-10. Mass spectra of HVA after electrooxidation for 0 (A), 5 (B), 15 (C), 30 (D), 60 (E) min in 0.01 M ammonium acetate solution (pH 6.70).

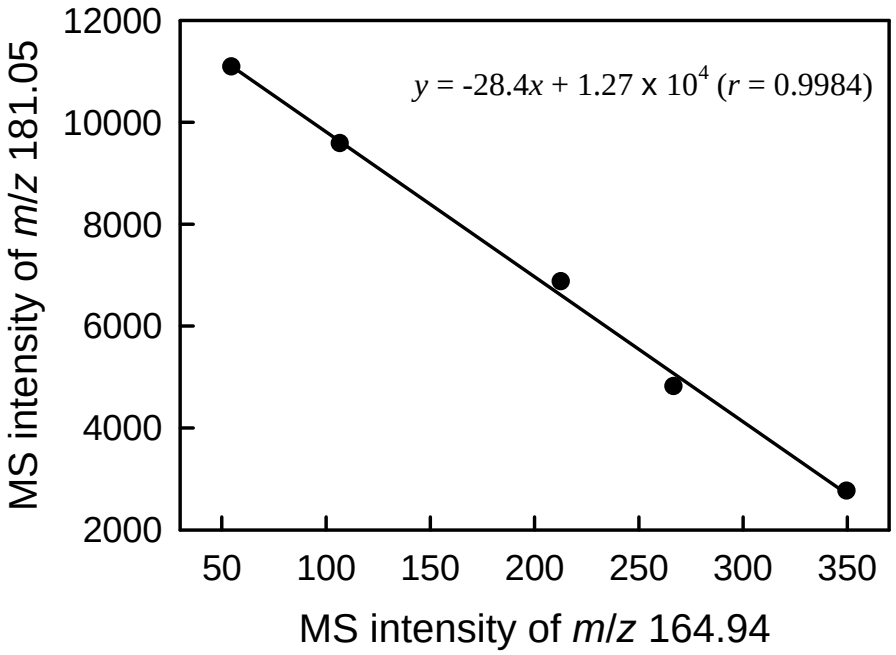

Fig. S-11. The plot of the intensity of *m*/*z* 181.05 versus *m*/*z* 164.94.

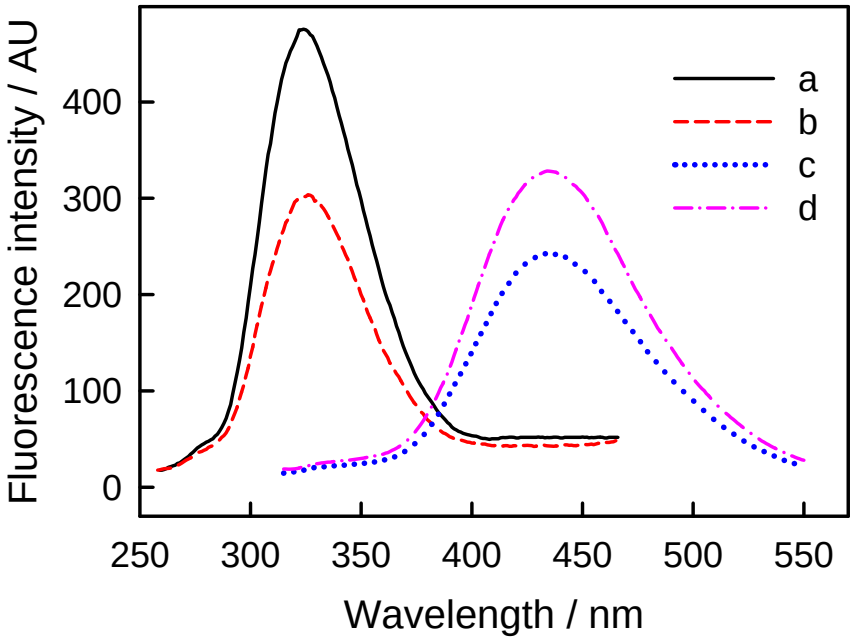

Fig. S-12. Fluorescence emission spectra of 100 μM HVA (a, black solid curve), HVA after 30 min electrooxidation (b, red dashed curve) and then added with 1.45 mg L^{-1} horseradish peroxidase and 7.18 × 10^{-4} M hydrogen peroxide (c, blue dotted curve), and 100 μM HVA directly mixed with 1.45 mg L^{-1} peroxidase and 7.18 × 10^{-4} M hydrogen peroxide (d, pink dashed dotted curve) in 0.01 M ammonium acetate solution (pH 6.70). Excitation wavelength: 294 nm.

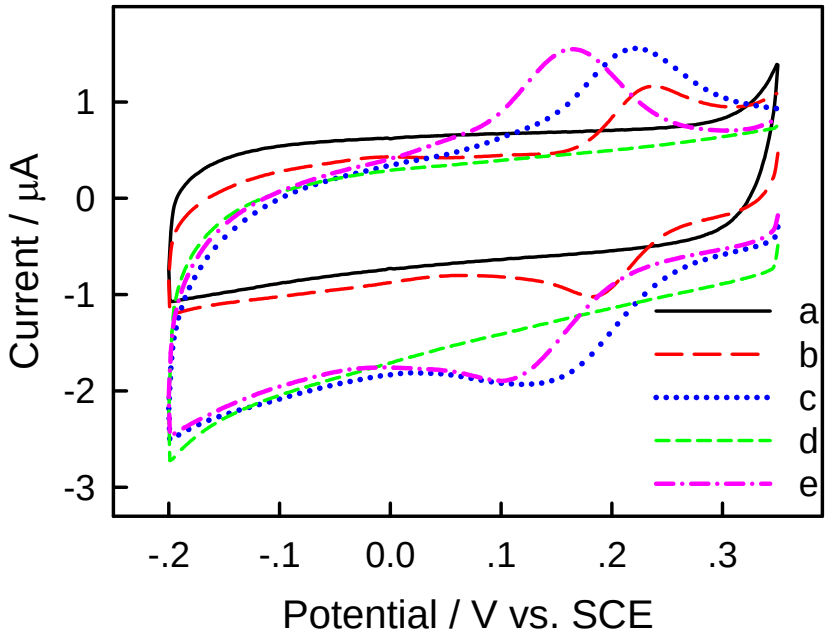

Fig. S-13. Cyclic voltammograms of 100 μM HVA (a, black solid curve), 100 μM HVA after 30 min electrooxidation (b, red long dashed curve) and then added with 0.73 mg L^{-1} horseradish peroxidase and 3.59×10^{-4} M hydrogen peroxide (c, blue dotted curve), the mixture of 1.45 mg L^{-1} horseradish peroxidase and 7.18×10^{-4} M hydrogen peroxide (d, green short dashed curve) and then mixed with HVA (e, pink dashed dotted curve). Medium: 0.01 M ammonium acetate solution (pH 6.70). Scan rate: 100 mV s^{-1}.

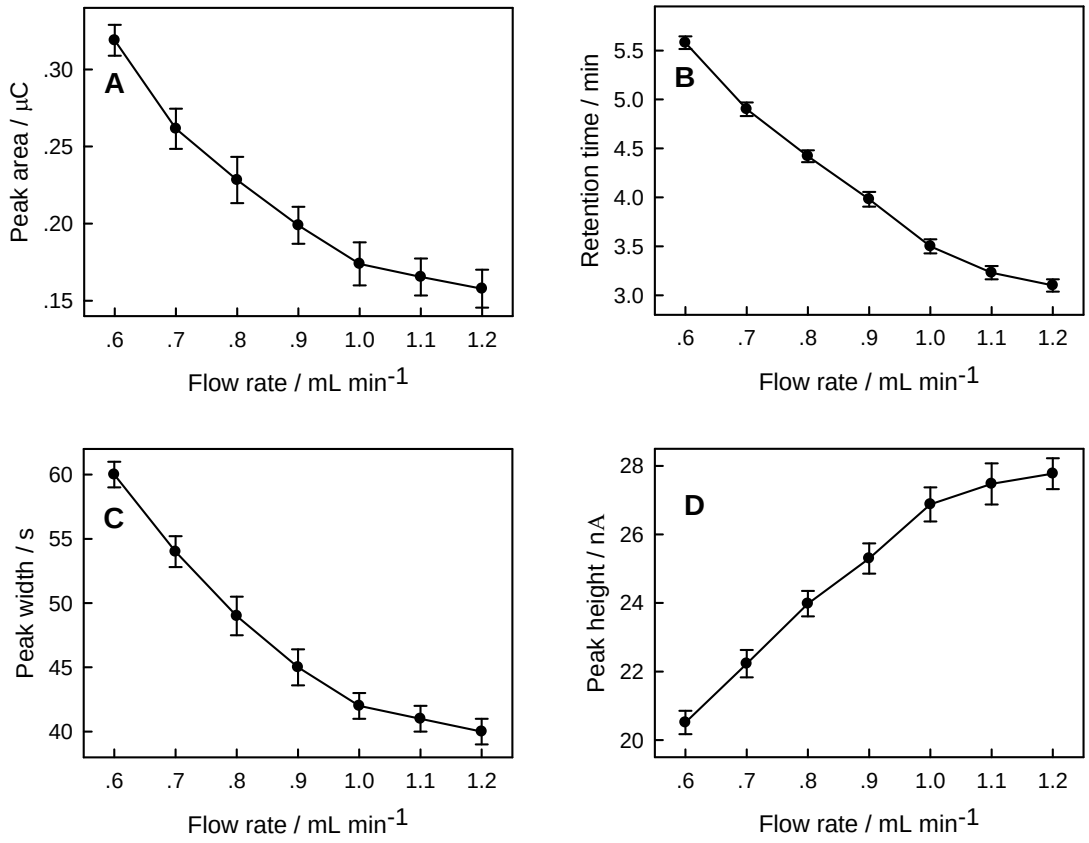

Fig. S-14. The dependences of the peak area, retention time, peak width as well as the peak height of DA on the flow rate using electrochemical detection at the bare GCE (3 mm in diameter). Chromatographic conditions are same as that in **Fig. S-9**, injected 20.0 μL standard solution with $c = 2.00 \times 10^{-6}$ mol L^{-1}, potential: +0.70 V.

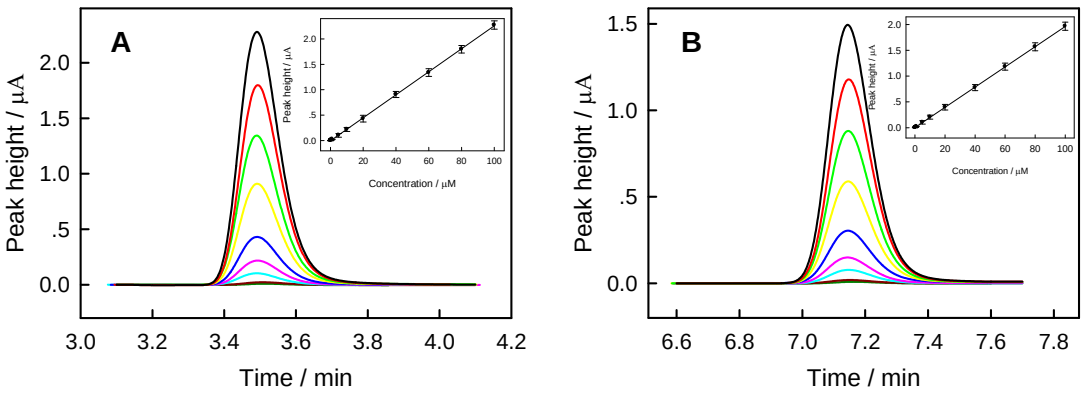

Fig. S-15. Chromatograms and corresponding calibration curves (Insert) of DA (A) and HVA (B) obtained with HPLC-ECD at the bare GCEs (5 mm in diameter). Chromatographic conditions are same as those in **Fig. S-14**, flow rate: 1.0 mL min^{-1}.

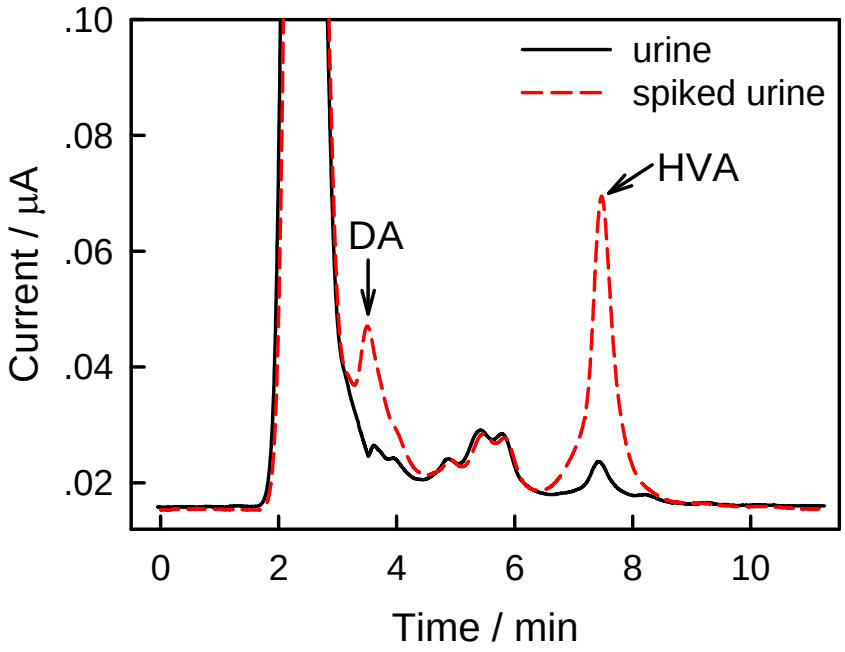

Fig. S-16. Typical chromatograms of a human urine sample (black solid curve) and the urine spiked with 2.00 μM DA and 10.0 μM HVA (red dashed curve) obtained by our HPLC-ECD at the bare GCE (5 mm in diameter). Chromatographic conditions are same as those in **Fig. S-15.**

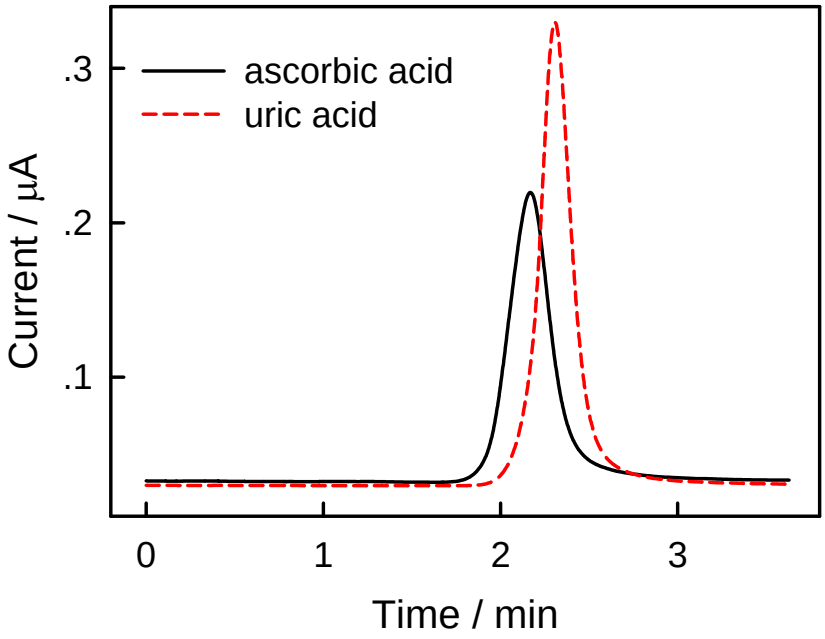

Fig. S-17. Chromatograms of 50.0 μM ascorbic acid (black solid curve) and uric acid (red dashed curve) obtained at the bare GCE (5 mm in diameter). Chromatographic conditions are same as those in **Fig. S-15**.

References (The numbering here is only for the Supporting Information)

1 X. Liu, B. Li and C. Li, *J. Serb. Chem. Soc.*, 2011, **76**, 113-123.

2 D. Tang, R. Yuan and Y. Chai, *Anal. Chem.*, 2008, **80**, 1582-1588.

3 J. Chen, M. A. Hamon, H. Hu, Y. Chen, A. M. Rao, P. C. Eklund and R. C. Haddon, *Science*, 1998, **282**, 95-98.

4 G. G. Guilbault, D. N. Kramer and E. B. Hackley, *Anal. Chem.*, 1967, **39**, 271-271.

5 G. G. Guilbault, P. J. Brignac and M. Zimmer, *Anal. Chem.*, 1968, **40**, 190-196.

6 Y. Li, M. Liu, C. Xiang, Q. Xie and S. Yao, *Thin Solid Films*, 2006, **497**, 270-278.

7 B. A. Patel, M. Arundell, K. H. Parker, M. S. Yeoman and D. O'Hare, *J. Chromatogr. B*, 2005, **818**, 269-276.

8 L. Lin, P. Qiu, L. Yang, X. Cao and L. Jin, *Anal. Bioanal. Chem.*, 2006, **384**, 1308-1313.

9 M. A. Fotopoulou and P. C. Ioannou, *Anal. Chim. Acta*, 2002, **462**, 179-185.

10 V. Carrera, E. Sabater, E. Vilanova and M. A. Sogorb, *J. Chromatogr. B*, 2007, **847**, 88-94.

11 N. Li, J. Guo, B. Liu, Y. Yu, H. Cui, L. Mao and Y. Lin, *Anal. Chim. Acta*, 2009, **645**, 48-55.

12 K. Vuorensola, H. Siren and U. Karjalainen, *J. Chromatogr. B*, 2003, **788**, 277-289.

13 M. Hadi and A. Rouhollahi, *Anal. Chim. Acta*, 2012, **721**, 55-60.

14 C. Xiao, X. Chu, Y. Yang, X. Li, X. Zhang and J. Chen, *Biosens. Bioelectron.*, 2011, **26**, 2934-2939.

15 S. Yang, G. Li, R. Yang, M. Xia and L. Qu, *J. Solid State Electrochem.*, 2011, **15**, 1909-1918.

16 M. A. Saracino, R. Mandrioli, L. Mercolini, A. Ferranti, A. Zaimovic, C. Leonardi and M. A. Raggi, *J. Pharm. Biomed. Anal.*, 2006, **42**, 107-112.

17 W. Zhang, Y. Xie, S. Ai, F. Wan, J. Wang, L. Jin and J. Jin, *J. Chromatogr. B*, 2003, **791**, 217-225.

18 L. Lionetto, A. M. Lostia, A. Stigliano, P. Cardelli and M. Simmaco, *Clin. Chim. Acta*, 2008, **398**, 53-56.

19 A. Garcia, M. Heinanen, L. M. Jimenez and C. Barbas, *J. Chromatogr. A*, 2000, **871**, 341-350.